

Effects of actuator nonlinearity on aeroelastic characteristics of a control fin

Won-Ho Shin^a, Seung-Jun Lee^a, In Lee^{a,*}, Jae-Sung Bae^b

^a*Division of Aerospace Engineering, Department of Mechanical Engineering, Korea Advanced Institute of Science and Technology, 373-1 Guseong-Dong, Yuseong-Gu, Daejeon 305-701, Republic of Korea*

^b*School of Aerospace and Mechanical Engineering, Korea Aerospace University, 200-1, Hwajeon-dong, Deogyang-gu, Goyang-City, Geonggi, Republic of Korea*

Received 29 May 2006; accepted 13 April 2007

Available online 2 July 2007

Abstract

The influences of actuator nonlinearities on actuator dynamics and the aeroelastic characteristics of a control fin were investigated by using iterative V-g methods in subsonic flows; in addition, the doublet-hybrid method (DHM) was used to calculate unsteady aerodynamic forces. The changes of actuator dynamics induced by nonlinearities, such as backlash or freeplay, and the variations of flutter boundaries due to the changes of actuator dynamics were observed. Results show that the aeroelastic characteristics can be significantly dependent on actuator dynamics. Thus, the actuator nonlinearities may play an important role in the nonlinear aeroelastic characteristics of an aeroelastic system. The present results also indicate that it is necessary to seriously consider the influence of actuator dynamics on the flutter characteristics at the design stage of actuators to prevent aeroelastic instabilities of aircraft or missiles.

© 2007 Elsevier Ltd. All rights reserved.

Keywords: Actuator nonlinearities; Aeroelastic characteristics; Actuator dynamics

1. Introduction

Consideration of static and dynamic aeroelastic phenomena is a significant issue in flight vehicle design. The corresponding unstable aeroelastic phenomena may cause the failure of flight vehicle structures or the decline of control performance. Hence, it is necessary to predict aeroelastic characteristics accurately in order to avoid aeroelastic instabilities during flight.

Recently, the control systems of wings have become more complex to improve flight performance. As actuators become more advanced, the effects of actuator dynamics on the aeroelasticity of flight vehicles become more significant. Aeroelastic analyses of flight vehicles are easily performed using an assumption of structural and aerodynamic linearity.

Nonlinear characteristics, particularly freeplay and backlash, and linear aeroelastic characteristics of flight vehicles or missile systems sometimes differ significantly from each other (Wooston et al., 1957; Laurenson and Tron, 1980), and aeroelastic behaviors that consider effects of an actuator on wing dynamics are considerably different from those that consider the wing only (Yehelzkely and Karpel, 1996).

*Corresponding author. Tel.: +82 42 869 3717; fax: +82 42 869 3710.

E-mail addresses: swh@asdl.kaist.ac.kr (W.-H. Shin), inlee@asdl.kaist.ac.kr (I. Lee), jsbae@kau.ac.kr (J.-S. Bae).

Nomenclature			
β	transmission error	J_m	moment of inertia of electric motor
δ	size of freeplay in load links	J_L	moment of inertia of load links
θ_m	rotational displacement of electric motor	k	stiffness between second gear and load links
θ_n	rotational displacement of second gear	k_i	stiffness of i th gear
θ_L	rotational displacement of load links	K_θ	linear static root stiffness
θ_1	rotational displacement of first gear	K_m	static stiffness of electric motor
Φ_F	modal matrix	K_L	static stiffness of load links
bl	size of backlash of gears	$\bar{\mathbf{K}}$	generalized stiffness matrix
c_i	damping of i th gear	$\bar{\mathbf{M}}$	generalized mass matrix
$\bar{\mathbf{C}}$	generalized damping matrix	N_i	i th gear reduction
C_m	damping of electric motor	N'_i	altering i th gear reduction
C_L	damping of load links	T	torque induced by electric motor
f_{flutter}	linear flutter frequency	T_L	transmission torque from second gear to load links
J_i	moment of inertia of i th gear	T_1	transmission torque from motor to first gear
		U_{flutter}	linear flutter velocity

McIntosh et al. (1981) performed experimental and theoretical studies of nonlinear flutter for a typical section model with hardening and softening spring along the hinge and plunge directions, and they observed limit-cycle and divergent amplitude-sensitive instabilities. Yang and Zhao (1988) studied the limit-cycle oscillations (LCO) of a typical section model with nonlinearity in the pitch direction subject to incompressible flow using the Theodorsen function. Lee (1986) developed an iterative scheme for multiple nonlinearities using the describing function method and the structural dynamics modification technique.

Lee and Tron (1989) carried out a flutter sensitivity study for a CF-18 aircraft with a wing-folding hinge and investigated the flutter characteristics and effects on limit-cycle flutter for the various wing-folding angles.

Lee and Kim (1995) studied LCO and chaotic motion of a missile control surface with freeplay using a time-domain analysis. Paek and Lee (1996) performed a flutter analysis for a launch vehicle control surface with control actuators and investigated the effect of the sweep angle on the flutter characteristics of a wing with dynamic stiffness. Conner et al. (1997) performed numerical and experimental studies on the nonlinear aeroelastic characteristics of a typical section wing with control surface freeplay. Liu and Chan (2000) investigated the LCO phenomenon for a nonlinear aeroelastic system under unsteady aerodynamics, and they showed that wind tunnel test results agreed well with predictions obtained both theoretically and numerically. Radcliffe and Cesnik (2001a, b) performed theoretical and experiment tests for the multi-hinged wings and checked the effect of nonlinearity on post-flutter flight speeds. Paek et al. (2002) studied the flutter characteristics of a wraparound fin while considering rolling motion and aerodynamic nonlinearity. Bae et al. (2002) used frequency-domain and time-domain analyses to study the subsonic nonlinear flutter characteristics of wings with a control surface. Librescu et al. (2003) performed a study of the benign and catastrophic characters of the flutter instability boundary of 2-D lifting surfaces in a supersonic flow field, and they studied the bifurcational behavior of an aeroelastic system near a flutter boundary using a method based on the first Liapunov method. Patil and Hodges (2004) investigated the importance of aerodynamic and structural geometrical nonlinearities in the aeroelastic behavior of high-aspect-ratio wings. Bae et al. (2004a) investigated the nonlinear aeroelastic characteristics of a deployable missile control fin, and showed that the aeroelastic characteristics can become more stable than in the case of linear aeroelasticity due to the nonlinearity of a deployable hinge. And Bae et al. (2004b) studied the nonlinear aeroelasticity of an aircraft wing with freeplay and bilinear nonlinearity and they observed three different types of LCOs over a wide range of airspeeds beyond the linear flutter boundary. Shearer and Cesnik (2007) studied a highly flexible vehicle, the HALE aircraft, which has geometrical nonlinearity, and checked the importance of modeling of the nonlinearity. Attar and Dowell (2005) proposed a reduced-order system ID approach to the modeling of nonlinear structural behavior in aeroelasticity. Many studies have considered nonlinear flutter; in contrast, nonlinear flutter analyses that consider the structural nonlinearity of an actuator have not yet been performed.

In this paper, the nonlinear aeroelastic characteristics of a missile fin with an actuator (shown in Fig. 1) are investigated with consideration of actuator nonlinearities as well as the actuator dynamics. Actuator nonlinearities, including backlash, freeplay, or transmission error, are present in the actuator, and the transfer function of the actuator is obtained via a rational function type comprised of system coefficients. The finite element method (FEM) is used for the free vibration analysis, and the doublet-hybrid method (DHM) (Ueda and Dowell, 1982), is used for the computation of subsonic unsteady aerodynamic forces. The fictitious mass (FM) method (Karpel and Newman, 1975) is used to reduce the computational effort.

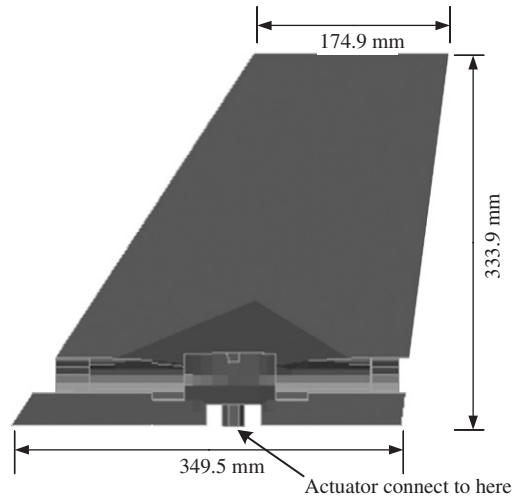


Fig. 1. The geometry of the missile fin.

2. Theoretical analysis

2.1. Actuator governing equation

Fig. 2 indicates the free-body diagram of the actuator, which consists of an electric motor, gears, and load links. The governing equation of the actuator can be obtained using Newton’s method at each point. The equation of motion can be represented as a combination of mass, damping, and stiffness of the motor at point A

$$J_m \ddot{\theta}_m + C_m \dot{\theta}_m + K_m \theta_m = T - T_1. \quad (1)$$

The governing equation of Gear 1 at point B can be written as

$$\frac{1}{N_1} \left\{ J_1 \ddot{\theta}_1 + c_1 (\dot{\theta}_1 - \dot{\theta}_n) + k_1 (\theta_1 - \theta_n) \right\} = T_1, \quad (2)$$

where

$$\theta_m = N_1 \theta_1. \quad (3)$$

Applying Eq. (3) to Eq. (2), the latter can be changed into

$$J_1 \frac{\ddot{\theta}_m}{N_1} = N_1 T_1 - c_1 \left(\frac{\dot{\theta}_m}{N_1} - \dot{\theta}_n \right) - k_1 \left(\frac{\theta_m}{N_1} - \theta_n \right). \quad (4)$$

The equation of motion at point C can be obtained as Eq. (5), and Eq. (2) can be represented as Eq. (6)

$$J_2 \ddot{\theta}_n + c_1 \left(\dot{\theta}_n - \frac{\dot{\theta}_m}{N_1} \right) + k_1 \left(\theta_n - \frac{\theta_m}{N_1} \right) = - \frac{T_L}{N_2}, \quad (5)$$

$$J_2 \ddot{\theta}_n = -c_1 \left(\dot{\theta}_n - \frac{\dot{\theta}_m}{N_1} \right) - k_1 \left(\theta_n - \frac{\theta_m}{N_1} \right) - \frac{T_L}{N_2}. \quad (6)$$

There is transmission error β between Gear 3 and the load axis that can be written as

$$\beta = \theta_1 - \theta_L = \frac{\theta_n}{N_2} - \theta_L. \quad (7)$$

The transmission torque can be represented as the product between stiffness and transmission error

$$T_L = k\beta. \quad (8)$$

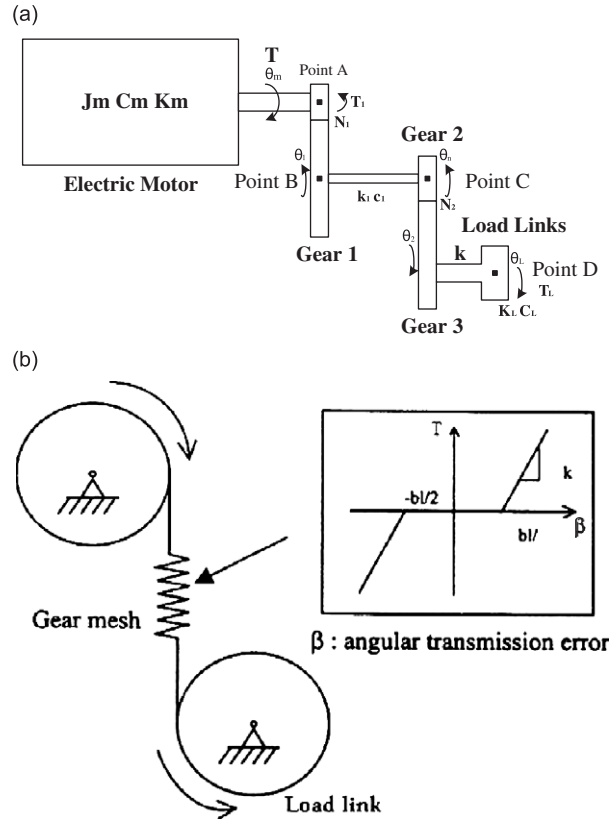


Fig. 2. The free-body-diagram and backlash model of the gear system. (a) The free body diagram of gear systems and (b) backlash model of the gear system.

The equation of motion at point D can be obtained as

$$J_L \ddot{\theta}_L + C_L \dot{\theta}_L + K_L \theta_L = T_L. \tag{9}$$

Assuming that the moments of inertia of gears are negligibly small and solving Eqs. (1)–(9), the relationship among θ_m , θ_n , and θ_L can be represented as

$$\theta_n = \left\{ \frac{N_2(J_L s^2 + C_L s + K_L)}{k} + N_2 \right\} \theta_L, \tag{10}$$

$$\theta_m = \left\{ \frac{N_2(J_L s^2 + C_L s + K_L)}{k} + N_2 + \frac{N_1(J_L s^2 + C_L s + K_L)}{N_2(c_1 s + k_1)} \right\} \theta_L. \tag{11}$$

Actuators may include several structural nonlinearities, such as backlash among the gears, freeplay of the load links, and transmission errors within the electric motor, gears, and load links. Such actuator nonlinearities may seriously affect the dynamic characteristics of a given actuator. Solving Eqs. (1)–(7), the transfer function of the actuator with transmission errors can be represented as

$$\frac{T(s)}{\theta_L(s)} = N_1 (J_m s^2 + C_m s + K_m) \left[\left\{ \frac{1}{N_2(k_1 + c_1 s)} + \frac{1}{k} \right\} (J_L s^2 + C_L s + K_L) + N_2 \right] + \frac{J_L s^2 + C_L s + K_L}{N_1 N_2}. \tag{12}$$

Freeplay and backlash nonlinearities of the actuator can be represented via a function between the nonlinear restoring force and the displacement, and they can be written as

$$f_{\text{backlash}}(\beta, bl) = \begin{cases} 0 & \text{for } |\beta| < bl \\ k(\beta - bl) & \text{for } |\beta| > bl. \end{cases} \tag{13a}$$

$$f_{\text{freeplay}}(\theta_L, \delta) = \begin{cases} 0 & \text{for } |\theta_L| < \delta \\ K_L(\theta_L - \delta) & \text{for } |\theta_L| > \delta \end{cases} \quad (13b)$$

where bl and δ are magnitudes of backlash and freeplay nonlinearities, respectively.

The equivalent stiffness of a nonlinear spring can be obtained using the general describing function method (Gelb and Velde, 1968), and the describing function of Eq. (13) can be written as

$$\psi_{\text{backlash}}(\beta, bl) = 1 - \frac{2}{\pi} \left[\sin^{-1} \frac{bl}{\beta} + \frac{bl}{\beta} \sqrt{1 - \left(\frac{bl}{\beta}\right)^2} \right], \quad (14a)$$

$$\psi_{\text{freeplay}}(\theta_L, \delta) = 1 - \frac{2}{\pi} \left[\sin^{-1} \frac{\delta}{\theta_L} + \frac{\delta}{\theta_L} \sqrt{1 - \left(\frac{\delta}{\theta_L}\right)^2} \right]. \quad (14b)$$

The actuator is connected to the control fin, and the actuator operates as the boundary condition of the control fin. Hence, changes in actuator dynamics can influence the aeroelastic characteristics of the control fin.

2.2. Aeroelastic equations

The aeroelastic equations of the missile fin with concentrated structural nonlinearity, such as freeplay and backlash, can be written as

$$\mathbf{M}\ddot{\mathbf{u}} + \mathbf{C}\dot{\mathbf{u}} + \mathbf{K}_u(\omega, \mathbf{u})\mathbf{u} = \mathbf{F}(t, \mathbf{u}, \dot{\mathbf{u}}), \quad (15)$$

where \mathbf{M} , \mathbf{C} and \mathbf{u} are the mass matrix, damping matrix and displacement vector, respectively. In addition, $\mathbf{F}(t, \mathbf{u}, \dot{\mathbf{u}})$ is the unsteady aerodynamic force and $\mathbf{K}_u(\omega, \mathbf{u})$ is the nonlinear stiffness matrix. The nonlinear stiffness matrix is divided into linear and nonlinear terms, which can be written as

$$\mathbf{K}_u(\omega, \mathbf{u})\mathbf{u} = \mathbf{K}(\omega)\mathbf{u} + f(\omega, \mathbf{u}), \quad (16)$$

where $\mathbf{K}(\omega)$ is a dynamic stiffness matrix, and $f(\omega, \mathbf{u})$ is the restoring force vector. In an aeroelastic system with structural nonlinearity and dynamic stiffness, structural properties vary with the behavior of the system. Hence, the aeroelastic results may be inaccurate if the constant modal coordinate of the nominal model is used to reduce the computational time and memory. Also, it takes too much time to redefine the modal coordinates of the aeroelastic system as the structural properties vary. In addition, it might be meaningless to perform an aeroelastic analysis on generalized modal coordinates. For these reasons, the FM method is used to improve the accuracy and computational time while using generalized modal coordinates.

The FM method, suggested by Karpel (1975), is used to couple several substructures. The FM is added to interface coordinates between the actuator and the structure. The equation of motion-adding FM, \mathbf{M}_F , is rewritten as

$$(\mathbf{M} + \mathbf{M}_F)\ddot{\mathbf{u}} + \mathbf{C}\dot{\mathbf{u}} + \mathbf{K}\mathbf{u} = \mathbf{F}(t, \mathbf{u}, \dot{\mathbf{u}}). \quad (17)$$

The eigenvector and eigenvalue matrices are obtained by solving the eigenvalue problem of Eq. (17). When the modal matrix Φ_F of the FM model is used, the structural displacement vector can be transformed into modal coordinates as follows:

$$\mathbf{u} = \Phi_F \boldsymbol{\eta}, \quad (18)$$

where $\boldsymbol{\eta}$ is the displacement vector in modal coordinates. Then, the generalized aerodynamic forces can be written as

$$\bar{\mathbf{F}} = \Phi_F^T \mathbf{F} = \mathbf{q} \Phi_F^T \mathbf{Q} \Phi_F \boldsymbol{\eta} = \mathbf{q} \bar{\mathbf{Q}} \boldsymbol{\eta}, \quad (19)$$

where \mathbf{q} and $\bar{\mathbf{Q}}$ are the dynamic pressure and the generalized aeroelastic coefficient matrix, respectively. On the other hand, the governing equation of the real structure induced by actuator nonlinearity and dynamics, $\Delta \mathbf{K}(\omega, \mathbf{u})$, is written as

$$\mathbf{M}\ddot{\mathbf{u}} + \mathbf{C}\dot{\mathbf{u}} + (\mathbf{K} + \Delta \mathbf{K})\mathbf{u} = \mathbf{F}(t, \mathbf{u}, \dot{\mathbf{u}}). \quad (20)$$

Therefore, Eq. (20) can be rewritten as

$$(\bar{\mathbf{M}} - \Phi_F^T \mathbf{M}_F \Phi_F) \ddot{\boldsymbol{\eta}} + \bar{\mathbf{C}} \dot{\boldsymbol{\eta}} + (\bar{\mathbf{K}} + \Phi_F^T \Delta \mathbf{K}(\omega, \mathbf{u}) \Phi_F) \boldsymbol{\eta} = \mathbf{q} \bar{\mathbf{Q}} \boldsymbol{\eta} - \Phi_F^T f(\omega, \mathbf{u}). \quad (21)$$

Although $\Delta\mathbf{K}(\omega, \mathbf{u})$ has various values, $\Phi_{\mathbf{F}}$ is consistently used to construct the generalized coordinate. The aerodynamics need not be calculated again to perform the free vibration analysis when structural changes occur. The FM method is an efficient and simple method to perform the aeroelastic analysis for the nonlinear structure.

3. Results and discussion

3.1. Actuator and control fin details

The geometric shape of a control fin, which has been determined for aeroelastic analyses, consists of upper and lower fins and can be deployed to reduce storage space, as shown in Fig. 1. The upper fin is made of aluminum alloy; the lower fin is made of steel. The upper fin is folded on mounting, and then unfolded after launching. Structural nonlinearity at the joint between the upper and lower fin may also affect the aeroelastic characteristics, and the ratio between the root rotation stiffness and the folding stiffness is significant for determining the flutter boundary (Bae et al., 2004a). However, in this study, only the effects of the structural nonlinearities of an actuator on the flutter boundaries were investigated, and thus the structural nonlinearities of a control fin were excluded.

The control fin is connected to an actuator, which consists of an electric motor, gears, and load links. The electric motor used in this study has static friction of 0.0028 N m and an armature resistance of 9.52 Ω ; additionally, the motor torque constant, back-emf, and motor inertia are 0.039 N m/A, 0.055 V/rads, and 4.5×10^{-6} kg m², respectively. The system parameters of the electric motor are listed in Table 1. The first and second reductions of the gear trains are 5.95

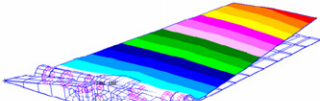
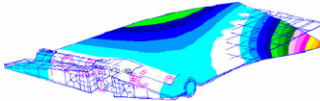
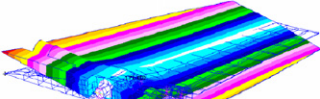
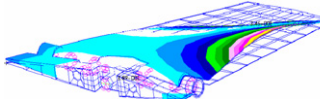
Table 1
Motor parameters of LC38RM-009-200 made by Copal Co

Static friction	F_m	0.0028 N m
Armature resistance	R_m	9.52 Ω
Motor torque constant	K_t	0.039 N m/A
Back_emf	K_b	0.055 V/rad/s
Motor inertia	J_m	4.5×10^{-6} kg m ²

Table 2
Gear train's mechanical parameters

Torsional stiffness of motor axis	k_1	74.3 N m/rad
Torsional stiffness of load axis	k_2	6120 N m/rad
Moment of inertia of motor	J_m	4.5×10^{-6} kg m ²
Total moment of inertia of load	J_L	0.0833 kg m ²
First reduction gear ratio	N_1	5.95
Second reduction gear ratio	N_2	8.69

Table 3
Natural frequencies and mode shape of the control fin using fictitious mass method

1st mode		3rd mode	
	Folding mode: 48.12 Hz		1st bending mode: 304.6 Hz
2nd mode		4th mode	
	Pitching mode: 159.0 Hz		1st torsion mode: 392.7 Hz

and 8.69. The total inertia moment of the load axis is 0.0833 kg m^2 , while the torsional stiffnesses of the motor and load axes are 74.3 N m/rad and 6.12 kN m/rad , respectively. The transfer functions of the actuator are represented with a combination of system parameters for the electric motor and gear trains. The mechanical parameters of the gear trains are listed in Table 2.

3.2. Nonlinear aeroelastic analysis

Aeroelastic analyses were performed for a control fin with an actuator (see Fig. 1) in linear and nonlinear missile systems using both a fictitious method and an iterative V-g method. Validations of the fictitious method and iterative V-g method used for the aeroelastic analyses were confirmed in previous studies (Bae et al., 2004a; Paek and Lee, 1996).

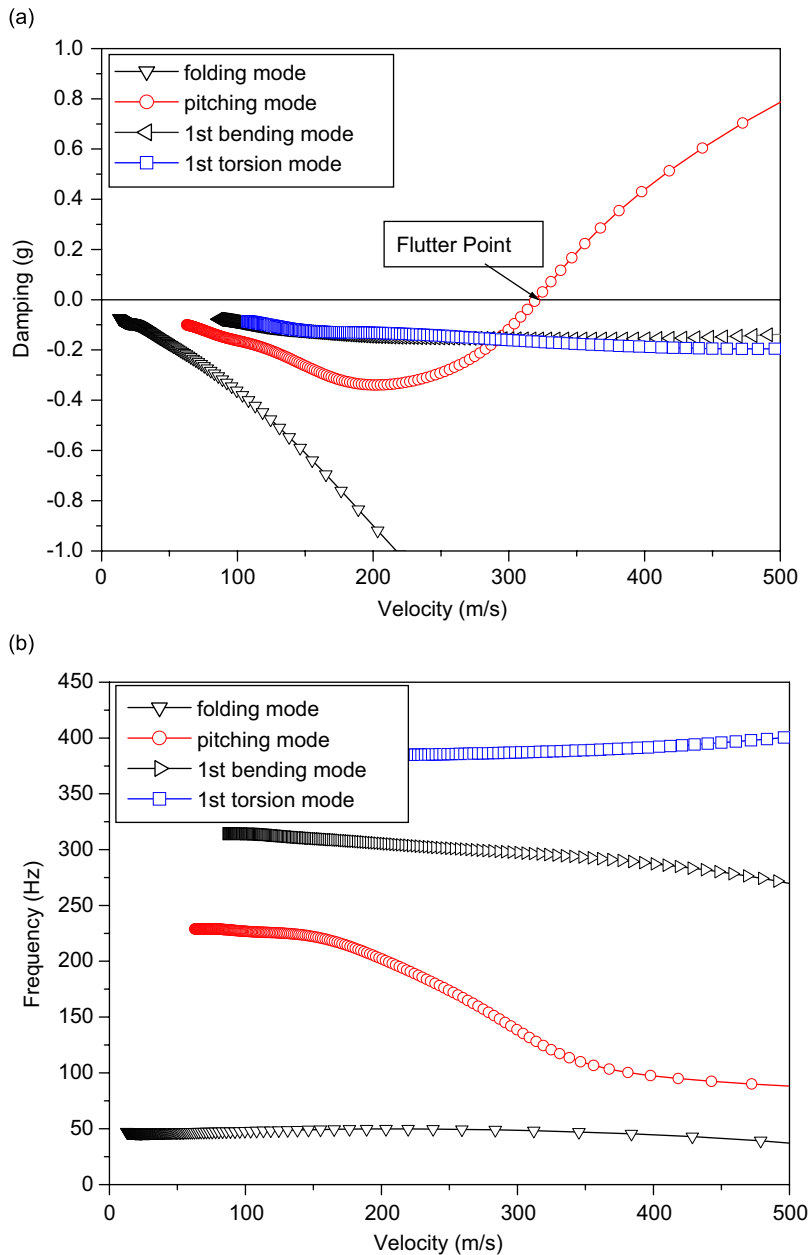


Fig. 3. Flutter analysis results of the control fin with the actuator using the iterative V-g method. (a) V-g graph and (b) V-F graph.

In the present study, the FEM was used for structural modeling of the control fin. Eight-node solid elements and bar elements were used to model the lower/upper fins and the hinge structures, respectively. Multipoint constraints were used to connect the lower/upper fins with the bar elements. A 1-D spring element for a root rotational spring was used, and point mass elements were used for the FM method. The root rotational spring indicated the boundary condition between the missile fin and the actuator. The free vibration analysis was performed using the FM method, and the first four natural frequencies and mode shapes are listed in Table 3. In addition, the generalized mass and stiffness matrices and the mode shape of the free vibration analysis were used for the aeroelastic analyses. The Mach number and air density used in the analyses were 0.7 and 1.23 kg/m^3 , respectively, and the subsonic unsteady aerodynamic forces were computed using DHM.

Flutter without actuator nonlinearity occurred as coalescence flutter between the folding and the pitching modes, as shown in Fig. 3. As the velocity increased, the pitching mode frequency decreased and the folding frequency increased. The two modes approached each other and then merged at the flutter point. The second mode was the pitching mode at the joints between the control fin and the actuator. In addition, the actuator nonlinearities affected the dynamic stiffness and the second mode frequency, and the second mode was the flutter mode that merged with the first mode. Hence, a change of the second mode frequency induced by the actuator nonlinearity may affect the flutter boundary. Flutter velocity and frequency without actuator nonlinearity were used as the reference flutter velocity, U_{ref} , and the reference flutter frequency, ω_{ref} .

For the case when the backlash nonlinearity is present in gears, Fig. 4 shows the changes of actuator dynamics, including the dynamic stiffness and the phase, according to the frequency ratio, which is normalized by the reference frequency, ω_{ref} . The damping ratio of the load links, ζ , was assumed to be 0.1, and the displacement was nondimensionalized by the magnitude of the freeplay. The ratios between the magnitudes of backlash and freeplay are assumed as $bl : \delta = 30 : 1$. The location of the under-peak point, the minimum, decreased as the effects of backlash nonlinearity increased. (The effect of nonlinearity is larger when the nondimensional displacement, θ_L/δ , is closer to 1; additionally, the displacement of the gear, θ_n , is obtained from Eq. (5).) The under-peak point, when the nondimensional displacement was 1.1, dropped to about 15% because of backlash nonlinearity, as compared to that without backlash.

Fig. 5 indicates that actuator dynamics changed according to the freeplay nonlinearity of the load links. The magnitude of dynamic stiffness for 1.1 of the nondimensional displacement decreased by 50% due to the influence of freeplay nonlinearity, compared to that without freeplay. However, the under-peak point did not change, in contrast to the previous case. Fig. 6 shows variations of actuator dynamics when the backlash nonlinearity and the freeplay nonlinearity were coupled. The magnitude and under-peak points decreased considerably as the effects of the actuator nonlinearity strengthened.

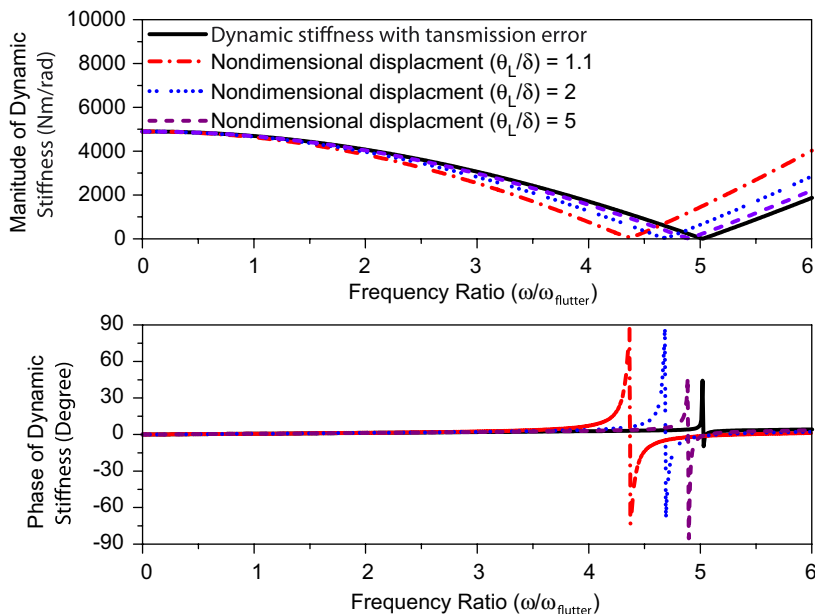


Fig. 4. Effects of backlash nonlinearity on the actuator dynamic characteristics. ($\zeta = 0.1$).

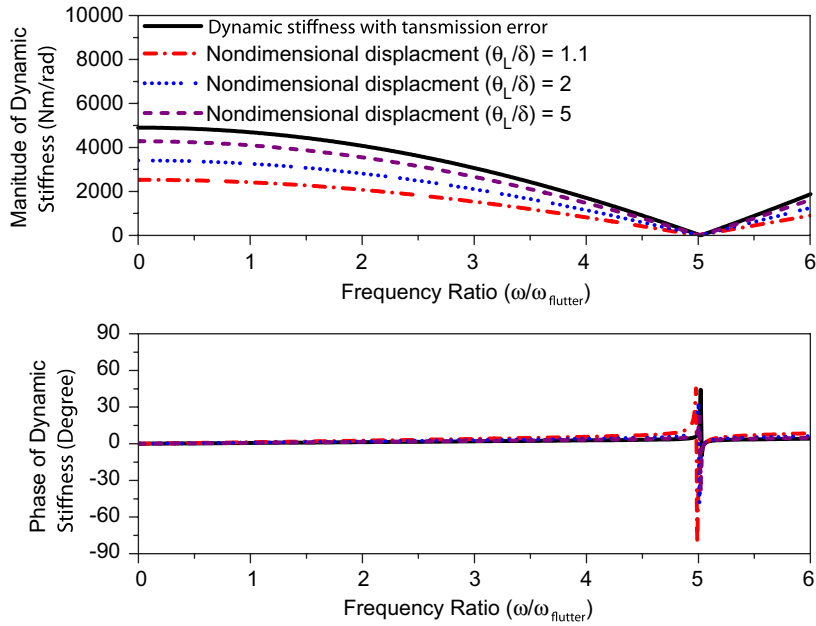


Fig. 5. Effects of freeplay nonlinearity on the actuator dynamic characteristics. ($\zeta = 0.1$).

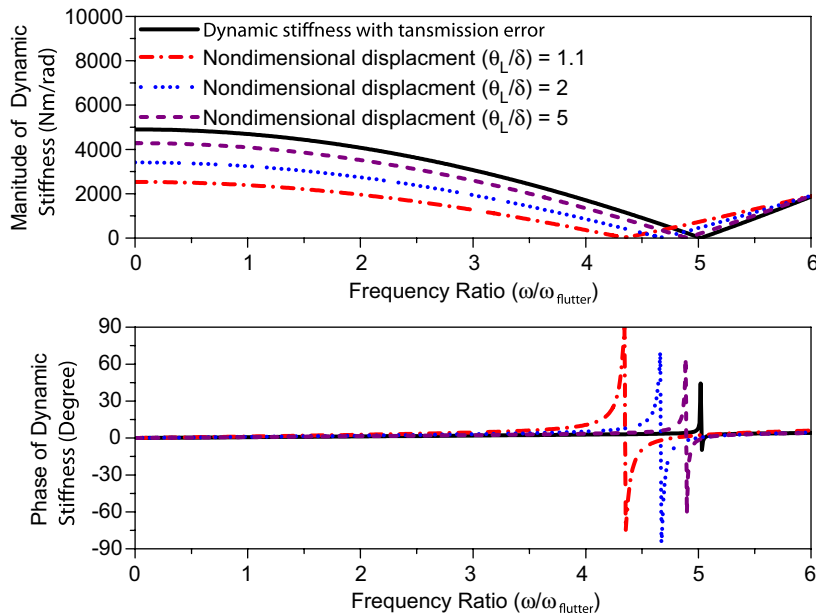


Fig. 6. Effects of both backlash and freeplay nonlinearity on the actuator dynamic characteristics. ($\zeta = 0.1$).

Fig. 7 shows that the flutter velocity ratio varied according to nondimensional displacement when the actuator nonlinearities are considered. In the case of backlash nonlinearity among the gears, the flutter speeds vary little as nondimensional displacements are changed, near $\theta/\delta = 1$. However, the flutter speed does not change according to nondimensional amplitudes of the oscillations, and converges to the reference flutter velocity in most nondimensional amplitude regions. The under-peak point without backlash nonlinearity, as shown in Fig. 4, was located above 5 (frequency ratio), and variations of dynamic stiffness were negligibly small near the reference frequency, whose

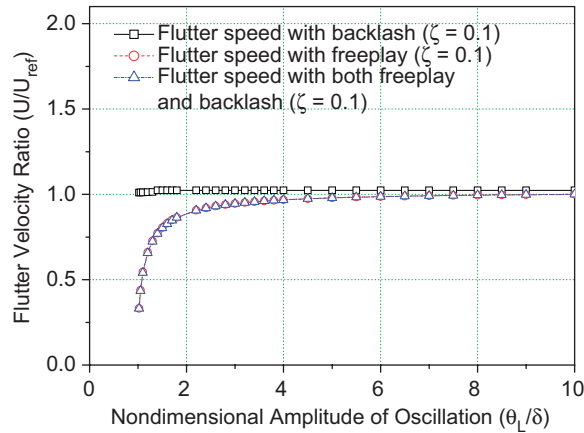


Fig. 7. Effects of actuator nonlinearities on flutter boundaries.

frequency ratio is 1. Hence, the results show that the effects of backlash nonlinearity on the flutter boundary may be negligible.

The flutter speeds, including the freeplay at load links, dropped as much as 60% in contrast to the previous case, wherein the nondimensional displacement approached 1. In addition, the flutter velocity ratio converged to 1 (which is the result obtained without actuator nonlinearities) as the nondimensional displacement increased. As shown in Fig. 5, the dynamic stiffness was reduced due to freeplay nonlinearity near the reference frequency, $\omega/\omega_{\text{ref}} = 1$, and then the flutter speed dropped considerably because of the decrements of dynamic stiffness. When the backlash and freeplay nonlinearities were coupled, the results were similar to the distribution of the flutter speed, including freeplay nonlinearity only. The effects of backlash nonlinearity were negligibly small near the reference frequency, where the freeplay nonlinearity had the main effect on the aeroelastic characteristics.

To investigate the effect of under-peak point locations on the flutter boundaries, the first and second reductions of gear trains were changed to thrice and twice, respectively. Figs. 8–10 show the changes of actuator dynamics according to the actuator nonlinearities after altering the first and second reductions. The under-peak point of dynamic stiffness moved to the near reference frequency, and the phase variation was small compared to the previous model. As shown in Fig. 8, the under-peak point decreased little according to nondimensional displacements, but the decrements of the under-peak point, induced by backlash nonlinearity, were negligible. Fig. 9 shows the effects of freeplay nonlinearity on actuator dynamics when the changed gear reductions are used. The magnitude of dynamic stiffness with 1.1 of the nondimensional displacement dropped to 50% because of the effects of freeplay nonlinearity, as compared to either with or without freeplay. Fig. 10 indicates that actuator dynamics, including both backlash and freeplay nonlinearities, were changed and the results were similar to those which considered only the freeplay nonlinearity. As the gear train reductions were altered, the influence of backlash nonlinearity on the actuator dynamics was weaker than when the original reductions were used.

Fig. 11 indicates that the flutter boundaries vary according to the actuator nonlinearities when the gear reductions of the actuator are changed in order to make the dynamic stiffness zero near the reference flutter frequency. As shown in Fig. 7, the flutter speeds which alter the gear reduction, have quite a different distribution from those using the original gear reductions. The flutter boundaries are decremented by 0.25 and observed in the regions where the nondimensional amplitudes of the oscillation are bigger than 2, including the backlash or freeplay nonlinearities, as compared with the reference flutter speed.

In the short region where the nondimensional amplitudes of the oscillation have a magnitude near 1, the nonlinear flutter occurs over the reference velocity; in addition, these phenomena are not observed when using the original gear reductions. In contrast to the results using the original gear reduction in Fig. 7, the flutter boundary with backlash only is significantly changed according to the nondimensional amplitude. In addition, the flutter boundaries, including both backlash and freeplay nonlinearities, differ significantly from those which consider freeplay only, since the backlash and the freeplay are coupled.

The nondimensional amplitudes, where flutter occurs above the reference velocity, are located near 1 when the backlash and freeplay nonlinearities are considered independently; in contrast, those regions increase up to 2 with coupled backlash and freeplay nonlinearities. Fig. 11 indicates that the effects of the actuator nonlinearity can increase

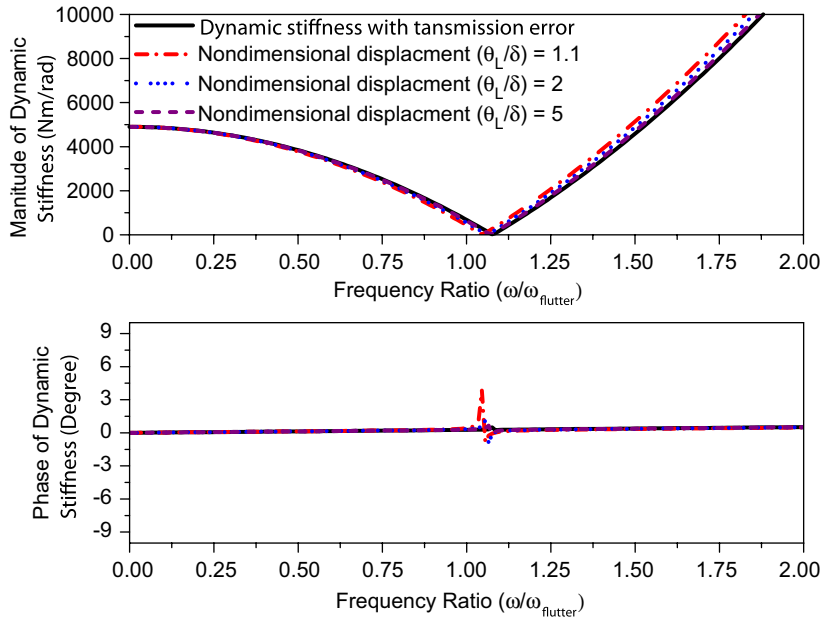


Fig. 8. Effects of backlash nonlinearity on the actuator dynamic characteristics using changed gear reductions. ($\zeta = 0.1, N'_1 = 3N_1, N'_2 = 2N_2$).

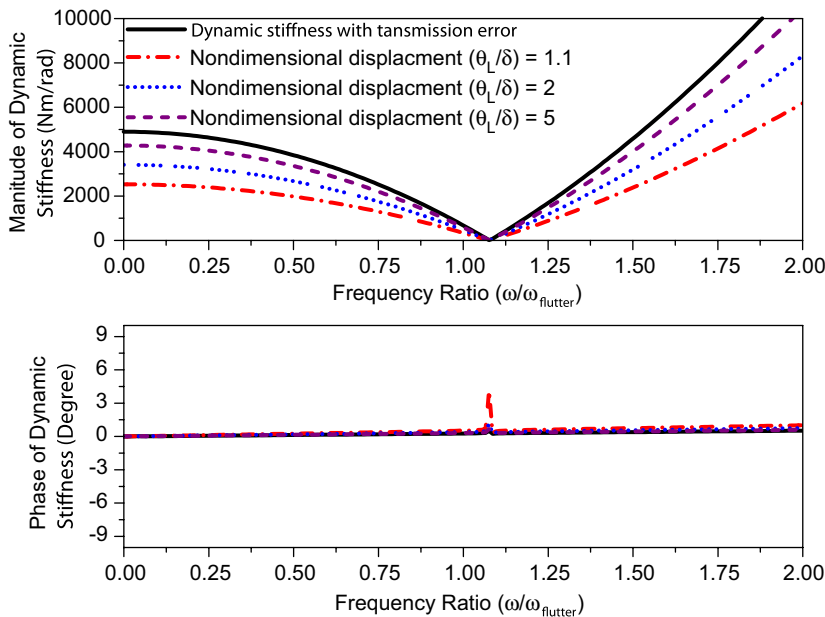


Fig. 9. Effects of freeplay nonlinearity on the actuator dynamic characteristics using changed gear reductions. ($\zeta = 0.1, N'_1 = 3N_1, N'_2 = 2N_2$).

aeroelastic boundaries in a specific region when the zero of the actuator is located near the flutter frequency. These results show that the actuator nonlinearity may affect the flutter boundary significantly, and that the flutter performance can change dramatically with the actuator dynamics, such as phase, peak and under-peak frequencies of the dynamic stiffness. Hence, the influences of actuator nonlinearities on flutter characteristics should be seriously considered when designing missile and aircraft actuators.

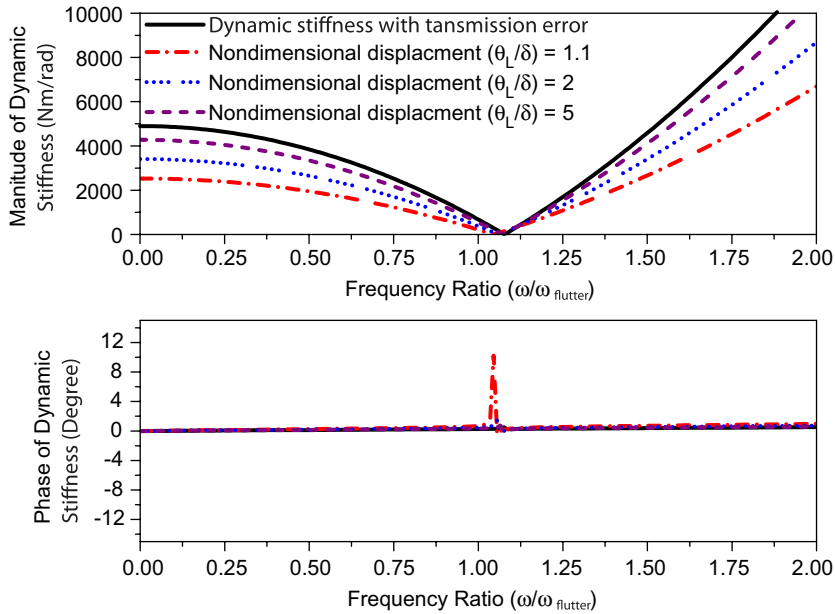


Fig. 10. Effects of both backlash and freeplay nonlinearity on the actuator dynamic characteristics using changed gear reductions. ($\zeta = 0.1, N'_1 = 3N_1, N'_2 = 2N_2$).

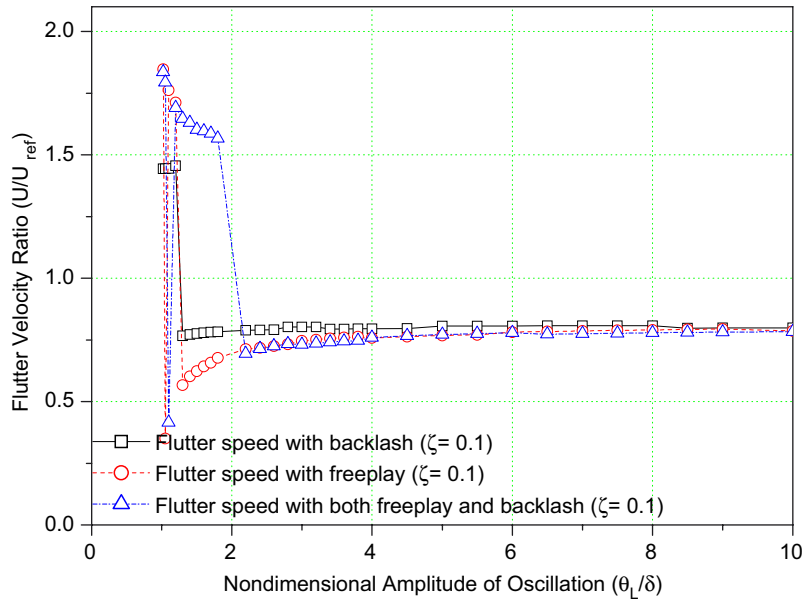


Fig. 11. Effects of actuator nonlinearities on flutter boundaries using changed gear reductions.

4. Concluding remarks

In this study, the influence of actuator nonlinearities on the aeroelastic characteristics of a control fin and actuator dynamics has been investigated by using iterative V-g methods in subsonic flows, and the unsteady aerodynamic force coefficients have been calculated by using the DHM based on a panel method. The actuator dynamics changes induced by actuator nonlinearities and gear reductions were investigated. The results show both that the freeplay can affect the

magnitude of dynamic stiffness and that the backlash may influence the poles or zeros of the dynamic stiffness. LCOs were observed both below and above the linear flutter speed, and the LCO characteristics of the aeroelastic system are significantly dependent on actuator nonlinearity as well as gear reductions. The aeroelastic boundary may decrease due to the actuator nonlinearities as compared to a linear case. In addition, the flutter boundary may improve, induced by the effects of the phase change when flutter occurs near the frequency of an actuator pole or zero. Thus, the actuator nonlinearities may play a significant role in the nonlinear flutter characteristics of an aeroelastic system. The results also indicate that it is necessary to seriously consider the actuator dynamics at the design stage in order to prevent aeroelastic instabilities of aircraft or missiles.

Acknowledgment

This research was supported by the Agency for Defense Development (ADD) in the Republic of Korea. This support is gratefully acknowledged.

References

- Attar, P.J., Dowell, E.H., 2005. A reduced order system ID approach to the modeling of nonlinear structural behavior in aeroelasticity. *Journal of Fluids and Structures* 21, 531–542.
- Bae, J.S., Yang, S.M., Lee, I., 2002. Linear and nonlinear aeroelastic analysis of a fighter-type wing with control surface. *Journal of Aircraft* 39 (4), 697–708.
- Bae, J.S., Kim, D.K., Shin, W.H., Lee, I., Kim, S.H., 2004a. Nonlinear aeroelastic analysis of a deployable missile control fin. *Journal of Spacecraft and Rockets* 41 (1), 264–271.
- Bae, J.S., Inman, D.J., Lee, I., 2004b. Effects of structural nonlinearity on subsonic aeroelastic characteristics of an aircraft wing with control surface. *Journal of Fluids and Structures* 19 (6), 747–763.
- Conner, M.D., Tang, D.M., Dowell, E.H., Virgin, L.N., 1997. Nonlinear behavior of a typical airfoil section with control surface freeplay: a numerical and experimental study. *Journal of Fluids and Structures* 11 (1), 89–109.
- Gelb, A., Velde, W.E.V., 1968. *Multiple-Input Describing Functions and Nonlinear System Design*. McGraw-Hill, New York.
- Karpel, M., Newman, M., 1975. Accelerated convergence for vibration modes using the substructure coupling method and fictitious coupling masses. *Israel Journal of Technology* 13, 55–62.
- Laurenson, R.M., Tron, R.M., 1980. Flutter analysis of missile control surface containing structural nonlinearities. *AIAA Journal* 18 (12), 1245–1251.
- Lee, C.L., 1986. Iterative procedure for nonlinear flutter analysis. *AIAA Journal* 24 (5), 833–840.
- Lee, B.H.K., Tron, A., 1989. Effects of structural nonlinearities on flutter characteristics of the CF-18 aircraft. *Journal of Aircraft* 26 (8), 781–786.
- Lee, I., Kim, S.H., 1995. Aeroelastic analysis of a flexible control surface with structural nonlinearity. *Journal of Aircraft* 32 (4), 868–874.
- Librescu, L., Chiochia, G., Marzocca, P., 2003. Implications of cubic physical/aerodynamic non-linearities on the character of the flutter instability boundary. *International Journal of Non-Linear Mechanics* 38, 173–199.
- Liu, J.K., Chan, H.C., 2000. Limit cycle oscillations of a wing section with a tip mass. *Nonlinear Dynamics* 23, 259–270.
- McIntosh Jr., S.C., Reed Jr., R.E., Rodden, W.P., 1981. Experimental and theoretical study of nonlinear flutter. *Journal of Aircraft* 18 (12), 1057–1063.
- Paek, S.K., Lee, I., 1996. Flutter analysis for control surface of launch vehicle with dynamic stiffness. *Computers & Structures* 60 (4), 593–599.
- Paek, S.H., Bae, J.S., Lee, I., 2002. Flutter analysis of a wraparound fin projectile considering rolling motion. *Journal of Spacecraft and Rockets* 39, 66–72.
- Patil, M.J., Hodges, D.H., 2004. On the importance of aerodynamic and structural geometrical nonlinearities in aeroelastic behavior of high-aspect-ratio wings. *Journal of Fluids and Structures* 19, 905–915.
- Radcliffe, T.O., Cesnik, C.E.S., 2001a. Aeroelastic response of multi-segmented hinged wings. *Proceedings of the 42nd Structures, Structural Dynamics, and Material Conference, Seattle, Washington, DC, April 16–19, AIAA Paper 2001–1371*.
- Radcliffe, T.O., Cesnik, C.E.S., 2001b. Aeroelastic behavior of multi-hinged wings. *International Forum on Aeroelasticity and Structural Dynamics, Madrid, Spain, June 5–7*.
- Shearer, C. M., Cesnik, C.E.S., 2007. Nonlinear flight dynamics of very flexible aircraft. *Journal of Aircraft*, in press.
- Ueda, T., Dowell, E.H., 1982. A new solution method for lifting surfaces in subsonic flow. *AIAA Journal* 20 (3), 348–355.
- Wooston, D.S., Runyan, H.W., Andrews, R.E., 1957. Some effects of system nonlinearities in the problem of aircraft flutter. *NASA TN 3539*.
- Yang, Z.C., Zhao, L.C., 1988. Analysis of limit cycle flutter of an airfoil in incompressible flow. *Journal of Sound and Vibration* 123 (1), 1–13.
- Yehelzkely, E., Karpel, M., 1996. Nonlinear flutter analysis of missiles with pneumatic fin actuators. *Journal of Guidance, Control, and Dynamics* 19 (3), 664–670.